PHYSICS

Emergence of topological semimetals in gap closing in semiconductors without inversion symmetry

Shuichi Murakami,[1,2]* Motoaki Hirayama,[1,2] Ryo Okugawa,[1] Takashi Miyake[3]

A band gap for electronic states in crystals governs various properties of solids, such as transport, optical, and magnetic properties. Its estimation and control have been an important issue in solid-state physics. The band gap can be controlled externally by various parameters, such as pressure, atomic compositions, and external field. Sometimes, the gap even collapses by tuning some parameter. In the field of topological insulators, this closing of the gap at a time-reversal invariant momentum indicates a band inversion, that is, it leads to a topological phase transition from a normal insulator to a topological insulator. We show, through an exhaustive study on possible space groups, that the gap closing in inversion-asymmetric crystals is universal, in the sense that the gap closing always leads either to a Weyl semimetal or to a nodal-line semimetal. We consider three-dimensional spinful systems with time-reversal symmetry. The space group of the system and the wave vector at the gap closing uniquely determine which possibility occurs and where the gap-closing points or lines lie in the wave vector space after the closing of the gap. In particular, we show that an insulator-to-insulator transition never happens, which is in sharp contrast to inversion-symmetric systems.

INTRODUCTION

In electronic band theory of crystals, degeneracy at each wave vector $\mathbf{k}$ is understood in terms of symmetry. A dimension of an irreducible representation (irrep) of a k-group at a given $\mathbf{k}$ point is equal to degeneracy at the $\mathbf{k}$ point considered. For example, a fourfold degeneracy of valence bands at the Γ point in cubic semiconductors comes from cubic symmetry. Meanwhile, proposals of topological semimetals have shown us other possibilities for band degeneracies, stemming from topology. In this topological semimetal, a band gap closes at generic $\mathbf{k}$ points, and this closing of the gap originates not from symmetry, but from topological reasons. There are various topological semimetals, such as Weyl, Dirac, and nodal-line semimetals. In Weyl semimetals (WSMs) (*1*–*4*), the band structure has three-dimensional (3D) nondegenerate Dirac cones. There are various proposals of materials for WSMs (*2*, *5*–*13*), some of which have been experimentally confirmed, such as TaAs (*14*–*16*). Because of topological properties of Weyl nodes (*1*, *17*, *18*), characteristic surface states called Fermi arcs arise (*2*, *19*–*21*). As another example of topological semimetals, a nodal-line semimetal (*22*–*35*) has line nodes along which the band gap closes. Because the emergence of topological degeneracy is accidental, the search for candidate materials realizing topological semimetals is still elusive.

Here, we consider physics of topological semimetals from a new perspective. We focus on the evolution of a band structure of a general inversion-asymmetric insulator by changing a single parameter, m, which can be any parameter in the Hamiltonian. We suppose that the gap closes at some value of the parameter m. We then prove that after a further change of the value of m (Fig. 1A), the system always becomes either (i) a nodal-line semimetal (Fig. 1B) or (ii) a WSM (Fig. 1C). We show that the space group of the crystal and the wave vector at the gap closing uniquely determines which possibility is realized and where the gap-closing points or lines are located after the closing of the gap. Here, we restrict ourselves to 3D spinful systems with time-reversal symmetry, that is, nonmagnetic systems with nonzero spin-orbit coupling (SOC). In particular, we find that an insulator-to-insulator (ITI) phase transition never occurs in any inversion-asymmetric systems. It is in sharp contrast to inversion-symmetric systems.

This work is motivated by the universal phase diagram (Fig. 2A) between a topological insulator (TI) and a normal insulator (NI) in three dimensions (*1*). Our result in the present paper indicates that when inversion symmetry is broken at a transition between different $\mathbb{Z}_2$ topological numbers (*36*, *37*), that is, between a strong topological insulator (STI) and an NI [or a weak topological insulator (WTI)], a WSM phase always appears, as was expected by Murakami (*1*). This theory can be applied to any inversion-asymmetric crystals, such as BiTeI under high pressure (*6*) and Te under pressure (*34*).

RESULTS

Setup of the problem

We consider a Hamiltonian matrix $H(\mathbf{k}, m)$, where $\mathbf{k}$ is a Bloch wave vector and m is an external parameter controlling the gap. Furthermore, we assume that a space group of the system remains the same for any values of m. To see how the gap closes, we assume that for $m < m_0$, the system is an insulator, and that at $m = m_0$, the gap closes at a wave vector $\mathbf{k} = \mathbf{k}_0$. We assume the Hamiltonian to be analytic with respect to $\mathbf{k}$ and m. Then, we expand the Hamiltonian in terms of $m - m_0$ and $\mathbf{q} \equiv \mathbf{k} - \mathbf{k}_0$, and retain some terms of lower order to see the evolution of the band structure for $m > m_0$. For the purpose of application to real materials, we consider all the 138 space groups without inversion symmetry. For each space group, there are various $\mathbf{k}$ points, such as Γ, X, and L. Each $\mathbf{k}$ point is associated with a k-group (little group), which leaves the $\mathbf{k}$ point unchanged. To focus on the closing of the gap, we retain only the lowest conduction band and the highest valence band, whose irreps of the k-group at $\mathbf{k}_0$ are denoted by R_c and R_v, respectively. In our analysis, we use the complete list of double-valued irreps of k-groups by Bradley and Cracknell (*38*).

Varieties of 138 space groups, $\mathbf{k}$ points for each space group, and irreps at each $\mathbf{k}$ point lead to numerous possibilities. Our theory in this paper exhausts all the cases; we can substantially reduce the number of possible cases by the following considerations. First, we can exclude cases with $\dim R_v \geq 2$ or $\dim R_c \geq 2$, that is, the cases where the valence

[1]Department of Physics, Tokyo Institute of Technology, 2-12-1 Ookayama, Meguro-ku, Tokyo 152-8551, Japan. [2]Tokodai Institute for Element Strategy, Tokyo Institute of Technology, 2-12-1 Ookayama, Meguro-ku, Tokyo 152-8551, Japan. [3]Research Center for Computational Design of Advanced Functional Materials, National Institute of Advanced Industrial Science and Technology, Tsukuba 305-8568, Japan.
*Corresponding author. Email: murakami@stat.phys.titech.ac.jp

or the conduction band at $\mathbf{k}_0$ has degeneracy; it is because the gap does not close at $\mathbf{k}_0$. The reason is the following: If dim $R_c \geq 2$ at $\mathbf{k}_0$, the energy of the conduction band does not have a minimum at this $\mathbf{k}_0$ point, because the degenerate states at $\mathbf{k}_0$ will split linearly away from $\mathbf{k}_0$ along a generic direction (see Fig. 3A). Therefore, the gap does not close at $\mathbf{k}_0$. A similar argument applies to the valence band. Thus, we can safely restrict ourselves to the cases with dim R_v = dim R_c = 1; hence, the effective model is described by a 2 × 2 Hamiltonian matrix, which drastically simplifies our analysis. In particular, among possible wave vectors $\mathbf{k}_0$, we exclude the time-reversal invariant momenta (TRIM), because the bands at the TRIM always have Kramers degeneracies.

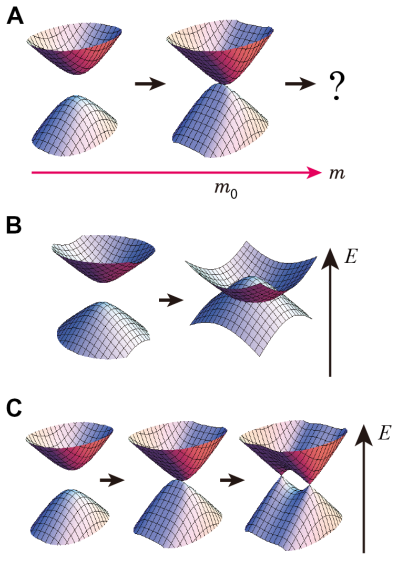

Fig. 1. Setup of the main problem of band evolution in an inversion-asymmetric semiconductor. (**A**) Band evolution toward gap closing. Schematic illustrations for two classes of band evolution into (**B**) a nodal-line semimetal, that is, semimetal with a gap closing along a loop, and (**C**) a WSM.

Various cases of gap-closing events classified by symmetry

Next, we determine the Hamiltonian matrix $H(\mathbf{k}, m)$ for each case from R_v and R_c. Resulting behaviors of the closing of the gap are then classified in terms of R_v and R_c. All the cases for the 138 space groups are summarized in the tables in the Supplementary Materials. Here, we briefly explain some representative cases of k-groups, and their details are given in Materials and Methods. In this analysis, in addition to point-group elements of a k-group, we have to consider symmetry operations of a form ΘO, where Θ is a time-reversal operator and O is a point-group element.

(i) No symmetry

We consider a generic $\mathbf{k}$ point having no special symmetry; namely, a k-group consists only of an identity operation. The band gap can close there, and the closing of the gap always accompanies a pair creation of Weyl nodes, as shown by Murakami and Kuga (*1*, *39*). This occurs because Weyl nodes are topological, having quantized monopole charges $q = \pm 1$ for the $\mathbf{k}$-space Berry curvature; this topological property allows for pair creation of Weyl nodes with $q = +1$ and -1. We call this case of Weyl-node creation "**1**," where **1** represents a number of monopole-antimonopole pairs (Fig. 3B).

(ii) C_2 symmetry

Suppose the k-group consists only of the twofold (C_2) symmetry. Then, there are two 1D irreps with opposite signs of the C_2 eigenvalues. Consequently, we have two cases: (ii-1) $R_c = R_v$ and (ii-2) $R_c \neq R_v$. For (ii-1) $R_c = R_v$, the gap cannot close by changing m because of level repulsion. On the other hand, for (ii-2) $R_c \neq R_v$, the gap can close because there is no level repulsion at $\mathbf{k}_0$, and we find that the closing of the gap accompanies the creation of a pair of Weyl nodes. When m is increased, the two Weyl nodes (a monopole and an antimonopole) move along the C_2 axis, as shown in Fig. 3C. We call this case "**1a**," where **1** represents the

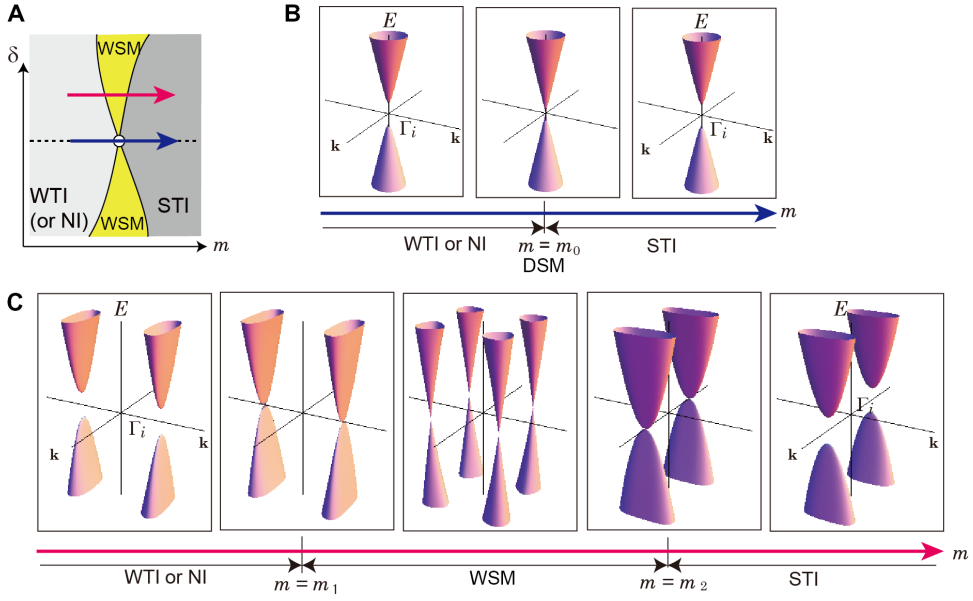

Fig. 2. Universal phase diagram for $\mathbb{Z}_2$ topological phase transitions and evolutions of the band structure upon the transition. (**A**) Universal phase diagram for $\mathbb{Z}_2$ topological phase transitions. It is shown as a function of an external parameter, m, and a parameter δ controlling a degree of inversion symmetry breaking (*1*). The horizontal dashed line is the inversion-symmetric line. (**B** and **C**) Evolutions of bulk band structure with a change of the parameter m for inversion-symmetric (B) and inversion-asymmetric (C) cases, respectively. The blue and the red arrows in (A) correspond to the cases (B) and (C), respectively. DSM represents a Dirac semimetal.

number of monopole-antimonopole pairs and **a** means "axial," that is, the relative direction between the two Weyl nodes is along a high-symmetry axis.

(iii) C_2 and ΘC_2 symmetries

The problem becomes more complicated when the time-reversal operator Θ is involved. Here, we consider a system with two C_2 symmetries C_{2y} and C_{2z}, whose rotational axes (y and z) cross perpendicularly. We focus on a $\mathbf{k}_0$ point lying on the C_{2z} axis, but not on the C_{2y} axis; the k-group thus consists of C_{2z} and ΘC_{2y}. There are two eigenvalues of C_{2z} with opposite signs, yielding two irreps, and R_c and R_v can take either of these two irreps. We consider two cases, (iii-1) $R_c = R_v$ and (iii-2) $R_c \neq R_v$, separately. For (iii-1) $R_c = R_v$, the closing of the gap leads to creations of two monopoles and two antimonopoles, and their trajectories are shown in Fig. 3D. As compared to (ii-1), the additional ΘC_{2y} symmetry suppresses level repulsion at $\mathbf{k}_0$, and therefore the gap can close. In our discussion, this behavior is called **2a**, where **2** means the number of monopole-antimonopole pairs and **a** means that the relative orientation between the two monopoles (and likewise, the two antimonopoles) is fixed to be along high-symmetry axes. For (iii-2) $R_c \neq R_v$, a pair of Weyl nodes is created, and they move along the C_{2z} axis as in (ii-2) (Fig. 3C). It is written as **1a**.

(iv) Mirror symmetry M

We consider the k-group consisting only of a mirror symmetry or a glide symmetry. There are two representations with opposite signs of mirror (or glide) eigenvalues. In the case (iv-1) $R_c = R_v$, the gap can close, leading to a creation of a pair of Weyl nodes. The trajectory of the monopole and that of the antimonopole are mirror images of each other. We call this pattern **1sa**, representing that the direction between the two Weyl nodes are always perpendicular to the mirror plane (Fig. 3E). The symbol **s** means that all the Weyl nodes are related by symmetry operations, and therefore, they are at the same energy. On the other hand, for (iv-2) $R_c \neq R_v$, the gap closes along a loop (that is, nodal line) within the mirror plane in **k** space. We call this case **1ℓ**, where **ℓ** stands for "loop" and **1** represents the number of loops. This degeneracy along the loop occurs because on the mirror plane, there is no level repulsion between the valence and the conduction bands belonging to the different irreps.

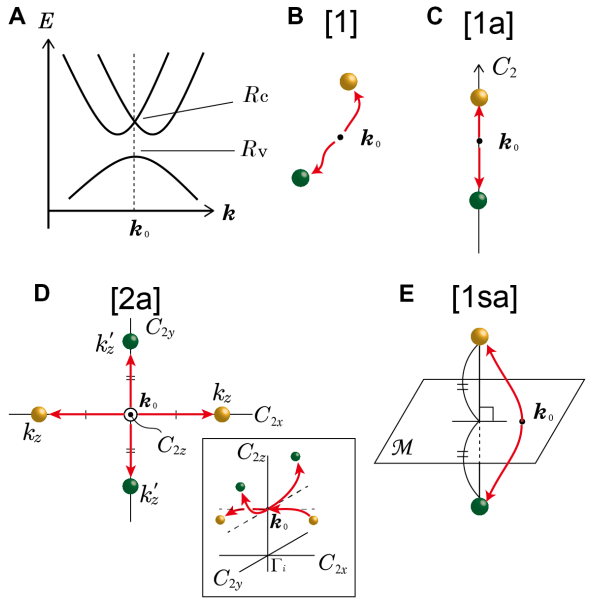

Fig. 3. Behavior of Weyl points at closing of the band gap in inversion-asymmetric insulators. (**A**) Schematic band structure for the case with dim $R_c = 2$ and dim $R_v = 1$. The gap does not close at $\mathbf{k}_0$ in this case. (**B**) Trajectory of Weyl nodes in the case (i) after pair creation at $\mathbf{k}_0$. (**C**) Trajectory of Weyl nodes in (ii-2) and in (iii-2). The Weyl nodes move along the C_2 axis. (**D**) Trajectory of Weyl nodes in the case (iii-1) viewed from different angles. The $\mathbf{k}_0$ point is on the C_{2z} axis away from a TRIM Γ_i. (**E**) Trajectory of Weyl nodes in the case (iv-1). In (B) to (E), yellow and green spheres denote monopoles and antimonopoles in **k** space, respectively, and they are both Weyl nodes.

One hundred thirty-eight inversion-asymmetric space groups

We can similarly calculate band structure evolution after the closing of the gap for all the high-symmetry points and lines for the 138 space groups without inversion symmetry. A complete list of all the cases is lengthy and is summarized in the tables in the Supplementary Materials. In Fig. 4, we summarize possible patterns for positions where the gap closes in **k** space for $m > m_0$, that is, after closing of the gap at $\mathbf{k}_0$. In the figure, the individual patterns are represented as **1sp**, **1ℓ**, and so on, and their notations are explained as follows. The numbers in Fig. 4 (B to Q) represent the number of pairs of Weyl nodes, except for **1ℓ**, **2ℓ**, **3ℓ**, **4ℓ**, and **6ℓ**, where the number represents the number of loops (nodal lines). The symbol **ℓ** means that there are nodal lines where the gap is closed. These nodal lines always appear on mirror planes and only when the valence and the conduction bands have different mirror eigenvalues. The symbol **a** (axial) denotes that the relative directions between the Weyl nodes are fixed to be along certain high-symmetry lines; meanwhile, the symbol **p** (planar) denotes that these directions are not confined along high-symmetry axes, but confined within high-symmetry planes. The symbol **c** (coplanar) denotes that all the monopoles and antimonopoles lie on the same high-symmetry plane. This symbol **c** is used only when there are more than one monopole-antimonopole pairs. The symbol **t** (tetrahedral) appears only for a few cases with tetrahedral or cubic symmetries. It means that four monopoles and four antimonopoles form eight vertices of a cube, whose center is a high-symmetry point, and four monopoles form a tetrahedron. The symbol **s** (symmetric) denotes that all the monopoles and the antimonopoles are related to each other by symmetry operations. In these cases, they are energetically degenerate, and it is possible to locate all the Weyl nodes on the Fermi energy. Otherwise, these monopoles and antimonopoles may not necessarily be at the same energy.

From this analysis, we conclude that there are only two possibilities after the closing of the gap in inversion-asymmetric insulators with time-reversal symmetry: nodal-line semimetals and WSMs. The nodal-line semimetals are denoted by $n\ell$ (n = 1, 2, 3, 4, and 6) (see Fig. 4A). Here, n is the number of nodal lines on mirror planes on which the highest valence and the lowest conduction bands have different mirror eigenvalues. The other possibility is the WSM, shown in Fig. 4 (B to Q). In some **k** with high symmetry, Weyl nodes and nodal lines are simultaneously generated. Remarkably, an ITI transition never occurs in the closing of the gap of the inversion-asymmetric insulators.

Materials realization

This universal result applies to any crystalline materials without inversion symmetry: Our first example is tellurium (Te), which has been theoretically shown to become a WSM at high pressure (*7*). Tellurium is a narrow-gap semiconductor without inversion symmetry, with its space group no.152 ($P3_121$) or no.154 ($P3_221$), which are mirror images of each other. At higher pressure, the gap closes and eventually a pair of

Weyl nodes is produced at each of the four P points on the K-H lines. The Weyl nodes then move along the threefold screw axes (K-H lines). According to our table, the only possibility of the gap closing is **1a**, in agreement with the above result. Moreover, this **1a** at the P points is allowed only when the C_3 eigenvalues of the valence and conduction bands are different; it was confirmed by the ab initio calculation (*7*).

The second example is $HgTe_xS_{1-x}$ under strain, which has been shown to become a WSM (*10*). It has a zinc blende structure (space group no. 216, $F\bar{4}3m$), but a strain along the [001] direction reduces the space group to no.119 ($I\bar{4}m2$). In this case, when x is increased from $x = 0$, the gap closes at four points on the Γ-K lines (Σ points) on the (110) and the $(1\bar{1}0)$ mirror planes, and then four pairs of Weyl nodes are created. The eight Weyl points then move within the $k_z = 0$ plane by a further increase of x until they mutually meet at Σ points and disappear after $\pm\pi/2$ rotation around the [001] axis (*10*). According to our table, the gap closing at each Σ point corresponds to **1sa**, meaning that the Weyl nodes move perpendicularly to the (110) or the $(1\bar{1}0)$ mirror planes, which agrees with the previous work (*10*).

Because degeneracies in topological semimetals are accidental, an efficient and systematic search of topological semimetals is difficult. Moreover, these degeneracies occur at generic **k** points; therefore, they may easily be overlooked in ab initio calculations, where band structure is usually calculated only along high-symmetry lines. Thus, a search of topological semimetals is an elusive issue.

Our results can be used for the search of topological semimetal materials. For example, we find that HfS has nodal lines near the Fermi level. HfS has a valley of the density of states near the Fermi level because of the following two reasons: One is that due to covalent bonds from S 3p orbitals, valence electrons in p orbitals tend to make a gap at the Fermi level to lower the total energy; it is prominent for atoms with large electronegativity. The other is an open shell of Hf 5d orbital ($5d^2$) having strong SOC. The structure of HfS is the same as that of tungsten carbide (WC) (Fig. 5A), with the space group no.187 ($P\bar{6}m2$) (*40*). Figure 5B shows the electronic band structure of HfS. If the SOC is neglected, Dirac nodal lines exist around the K points on the $k_z = 0$ plane. The SOC lifts the degeneracy of the Dirac nodal lines, and Weyl nodal lines appear instead, near the K points on the mirror plane $k_z = 0$. By applying pressure (Fig. 5C) or by atomic substitution from S to Se, the nodal lines become smaller. At 9 GPa, the nodal lines shrink to points (T points) on the K-Γ lines, and then the gap opens above 9 GPa. This evolution of the band structure corresponds to **1ℓ** in our table.

Next, we show LuSI as a WSM under pressure. The conduction and the valence bands originate from Lu 6s + 5d orbitals and S 3p (and I 5p) orbitals, respectively. The structure type of LuSI is GdSI (Fig. 5E), with the space group no.174 ($P\bar{6}$) (*41*). Each type of atom constitutes a distorted trigonal lattice, which displaces the gap away from the Γ point. Figure 5F shows the electronic structure of LuSI having a very narrow gap (<0.04 eV) near the M point. It becomes a WSM under pressure, as shown in Fig. 5G, with details shown in Materials and Methods. Six monopoles and six antimonopoles exist at the same energy because they are related by symmetry. By applying pressure, the band gap first closes at six generic points on the $k_z = 0$ plane, related to each other by sixfold

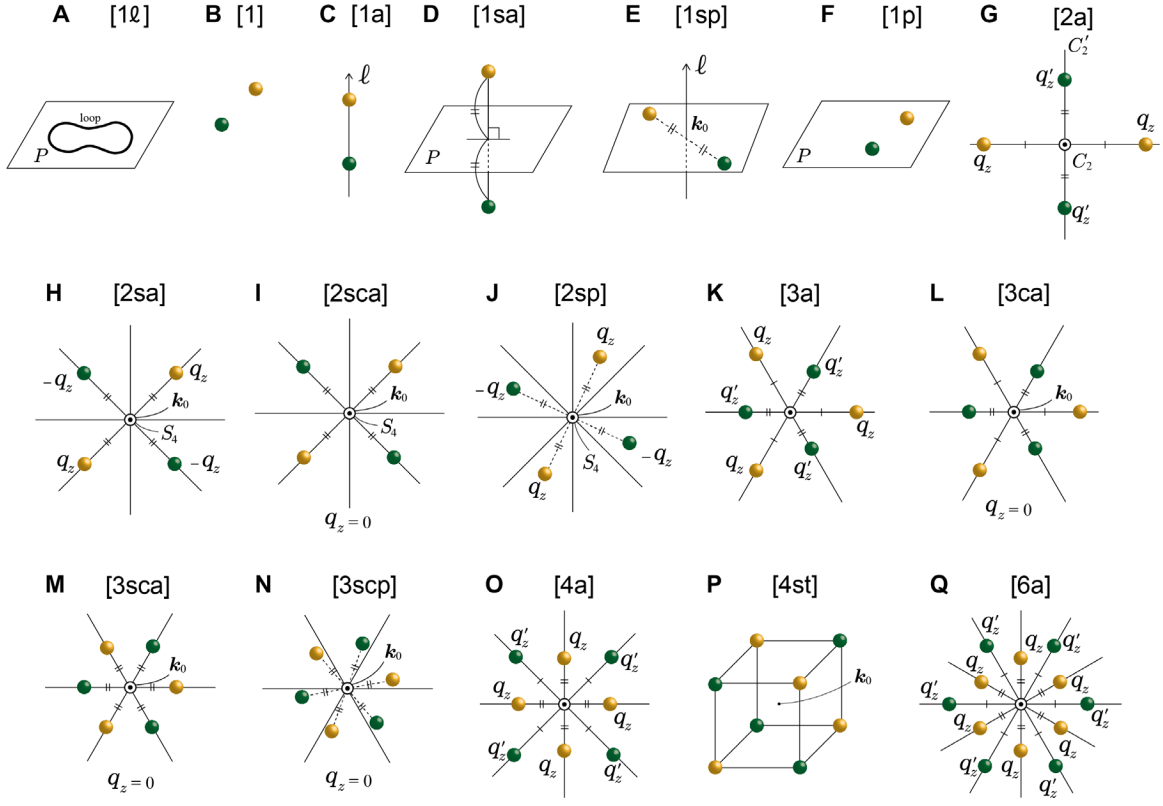

Fig. 4. All the patterns of locations of gap-closing points after parametric closing of the gap. (**A**) A line node for a nodal-line semimetal. Although the figure shows the case with a single line node, the number of line nodes can be 1, 2, 3, 4, or 6. (**B** to **P**) All the patterns of Weyl nodes after parametric gap closing at $\mathbf{k}_0$. Yellow and green spheres denote monopoles and antimonopoles in **k** space, and they are both Weyl nodes. Solid lines denote high-symmetry directions. In (G) to (O) and (**Q**), the z axis, taken to be perpendicular to the plane, is parallel to a high-symmetry axis. $\mathbf{q} \equiv \mathbf{k} - \mathbf{k}_0$ is the momentum measured from $\mathbf{k}_0$. In (I), (L), (M), and (N), all the Weyl nodes are coplanar with $\mathbf{k}_0$, whereas in (G), (H), (J), (K), (O), and (Q), the Weyl nodes are mutually displaced along the z direction.

symmetry. It corresponds to **1sa** because of the mirror symmetry M_z, belonging to the case (iv-1).

We show another example, MgPt, as a material having Weyl nodes. MgPt has the FeSi-type structure (Fig. 5I), having the space group no.198 ($P2_13$) (*42*). Figure 5 (J and K) shows the electronic structure of MgPt. The band near the Fermi level originates from Pt 5*d* orbitals having strong SOC. Weyl nodes w_1 and w_2 exist at general **k** points with no symmetry.

Topological phase transitions and $\mathbb{Z}_2$ topological number

Let us turn to $\mathbb{Z}_2$ phase transitions in three dimensions, that is, STI-NI (or STI-WTI) phase transitions. In the universal phase diagram (Fig. 2A) between an STI and an NI (or an WTI), there should be a finite region of a WSM phase when inversion symmetry is broken, as shown in the previous works (*1*, *39*); nevertheless, in its derivation (*1*), crystallographic symmetries, except for inversion symmetry, are not considered. The result in the present paper shows that this conclusion of existence of the WSM phase in the $\mathbb{Z}_2$ phase transition holds true in general, whenever inversion symmetry is broken. One of the remarkable conclusions here is that an ITI transition never occurs in inversion-asymmetric crystals. This is in strong contrast to inversion-symmetric systems, where a transition between different $\mathbb{Z}_2$ topological phases always occurs as an ITI transition (that is, at a single value of *m*), as seen in $TlBi(S_{1-x}Se_x)_2$ at around $x \sim 0.5$ (*43*, *44*).

We apply this theory to BiTeI, which lacks inversion symmetry (*45*), having the space group no.156 ($P3m1$). BiTeI is an NI at ambient pressure and has been proposed to become an STI at high pressure (*46*, *47*). Subsequently, ab initio calculations in previous work (*6*) showed existence of a WSM phase between the NI and the STI phases in a narrow window of pressure, which had been overlooked in some previous works (*46*, *47*). When the pressure is increased, the gap first closes at six *S* points on the *A*-*H* lines, and then six pairs of Weyl nodes are created. The six monopoles and six antimonopoles move in opposite directions; subsequently, they annihilate each other at generic points on three mirror planes, leading to the STI phase (*6*). Combination of all the trajectories of the Weyl nodes yields a loop around the TRIM point (*A* point); it means that a band inversion occurs at the *A* point between the low-pressure NI phase and the high-pressure STI phase and results in a subsequent change of the $\mathbb{Z}_2$ topological number (*1*, *39*). From our table, the space group no.156 at six *S* points gives **1sp**, meaning that immediately after the pair creations, they move perpendicularly to the *A*-*H* line, which is in agreement with the previous work (*6*).

Other examples are $LaBi_{1-x}Sb_xTe_3$ and $LuBi_{1-x}Sb_xTe_3$, which have been proposed to undergo an NI-WSM-TI phase transition by changing *x* (*6*). The space group is no.160 ($R3m$), lacking inversion symmetry. By increasing *x*, the band gap closes at six generic points, corresponding to creation of Weyl nodes (*6*). The resulting 12 Weyl nodes move in **k** space

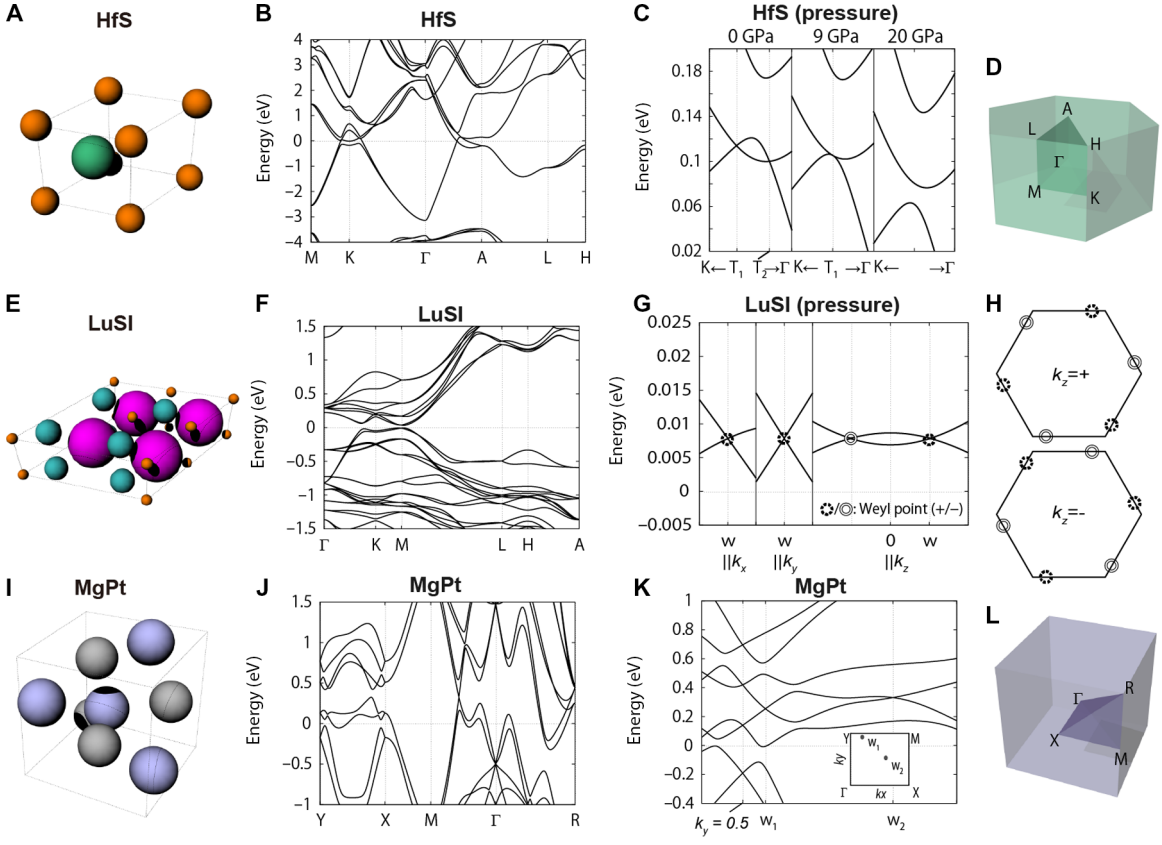

Fig. 5. Examples of proposed inversion-asymmetric topological semimetals found using the present theory. (**A**) Crystal structure of HfS. (**B** and **C**) Electronic band structure of HfS. (C) The phase transition of HfS under pressure. T_1 and T_2 are the points of the intersection of the nodal line with the *K*-Γ line. (**D**) Brillouin zone of HfS. (**E**) Crystal structure of LuSI. (**F**) Electronic band structure of LuSI. (**G**) Band structure of LuSI under pressure, where the lattice constant *c* is multiplied by 0.945. (**H**) Positions of the Weyl nodes of LuSI under pressure on the $k_z = 0$ plane. (**I**) Crystal structure of MgPt. (**J** and **K**) Electronic band structure of MgPt. (**L**) The Brillouin zone of LuSI and MgPt. The energy is measured from the Fermi level.

until they are annihilated at the six B ($\equiv\Sigma$) points. In our table, the B point corresponds to **1sp**, that is, the pair annihilation occurs between two Weyl nodes, which are moving perpendicularly to the normal direction of the mirror planes. It agrees with the previous work (*6*).

DISCUSSION

To summarize, we investigate the evolution of the band structure after parametric closing of the band gap in inversion-asymmetric crystals. We found that only two possibilities occur. One possibility is the WSM phase, and closing of the gap corresponds to monopole-antimonopole pair creations of Weyl nodes. Distribution of the Weyl nodes in $\mathbf{k}$ space after the closing of the gap is uniquely determined by symmetry. The other possibility is a nodal-line semimetal, with a gap closed along loops on mirror planes. From these results, we show that in any topological phase transitions with different $\mathbb{Z}_2$ topological numbers (without inversion symmetry), there should be a WSM phase between the two bulk-insulating phases. These results give us a systematic way to search materials for topological semimetals.

MATERIALS AND METHODS

Details of the first-principles calculation

The electronic structure was obtained from the local density approximation (LDA) of the relativistic density functional theory (DFT). Calculation of the electronic structure was performed using OpenMX code (www.openmx-square.org/) based on localized basis functions and norm-conserving pseudopotentials. We used 12 × 12 × 12 k-point sampling for HfS, HfSe, and MgPt, and 6 × 6 × 12 k-point sampling for LuSI. We used the experimental lattice parameters of these materials at ambient pressure (*40*–*42*). Lattice optimization for HfS under pressure is based on the LDA and was carried out using Quantum MAterials Simulator (QMAS) code (http://qmas.jp/) based on the projected augmented-wave method. We used 12 × 12 × 12 k-point sampling and 40 rydberg as a plane-wave energy cutoff in the lattice optimization. We also checked dynamic stability of HfS under pressure in the LDA of the density functional perturbation theory (DFPT) using Quantum ESPRESSO code (www.quantum-espresso.org/). We used 7 × 7 × 7 k-point sampling for the DFT and the DFPT calculations at ambient pressure and under 20 GPa. The structure is at least metastable up to 20 GPa, because there is no imaginary frequency in the phonon dispersion, as shown in the Supplementary Materials.

In LuSI, numerical error in the structural optimization is larger than the energy scale around the Weyl point at ambient pressure because of the extremely small energy gap of LuSI at ambient pressure. Therefore, in our calculation, we simply multiplied the lattice constant c by 0.945 instead of structural optimization. A realistic value of the transition pressure to the WSM phase is an open question. Nevertheless, because of the extremely small gap of LuSI at ambient pressure, the transition pressure was expected to be small; therefore, the lattice structure should remain stable even in the WSM phase.

Details of the effective-model calculation

It is convenient in the following analysis to expand the Hamiltonian as $H(\mathbf{q}, m) = \sum_{i=1}^{3} a_i(\mathbf{q}, m)\sigma_i$, where σ_i ($i = x, y, z$) are Pauli matrices, $\mathbf{q} = \mathbf{k} - \mathbf{k}_0$, and $\sigma_z = +1$ and -1 correspond to the conduction and the valence band, respectively. Here, we omitted the term proportional to an identity matrix because it does not affect the gap-closing event. Because the gap closes at $m = m_0$, $\mathbf{q} = 0$, we had $a_i(\mathbf{q} = 0, m = m_0) = 0$, where $i = 1, 2, 3$. We assumed that when $m < m_0$, the gap is open. In each case presented below, we examined whether the gap can close or not by counting a codimension, d_c, that is, the number of parameters to be tuned to close the gap. If the codimension is equal or lower than the number of tunable variables, the gap can close there; otherwise, the gap does not close.

(i) No symmetry

When there is no special symmetry at the $\mathbf{k}$ point, the Hamiltonian is not restricted by symmetry. The gap of the 2 × 2 Hamiltonian closes when $a_x = a_y = a_z = 0$; this condition determines a curve in the 4D space ($\mathbf{q}$, m). This curve goes through the point ($\mathbf{q} = 0, m = m_0$), but it does not exist in the $m < m_0$ region by assumption, and therefore, the curve has a minimum value of m at $m = m_0$ (Fig. 6A). Therefore, as the value of m increases, the gap-closing point appears at $\mathbf{q} = 0$ for $m = m_0$, and then it splits into two points (Weyl nodes) when m is further increased. It is a pair creation of a monopole and an antimonopole.

(ii) C_2 symmetry

Suppose $\mathbf{k}$ is invariant only by a twofold (C_2) rotation taken to be around the z axis. For (ii-1) $R_c = R_v$, the 2 × 2 Hamiltonian satisfies $H(q_x, q_y, q_z, m) = H(-q_x, -q_y, q_z, m)$, where $\mathbf{q} \equiv \mathbf{k} - \mathbf{k}_0$. In particular, at $\mathbf{k} = \mathbf{k}_0$, the above equation becomes trivial, imposing no constraint on the Hamiltonian. Therefore, the gap cannot close by changing a single parameter, m, because three conditions [$a_i(\mathbf{q} = 0, m) = 0$, ($i = x, y, z$)] cannot be simultaneously satisfied in general.

On the other hand, for (ii-2) $R_c \neq R_v$, the opposite signs of the C_2 eigenvalues lead to an equation $H(q_x, q_y, q_z, m) = \sigma_z H(-q_x, -q_y, q_z, m)\sigma_z$. In particular, for $q_x = q_y = 0$, we obtained $H(0, 0, q_z, m) = a_z(q_z, m)\sigma_z$, whose gap closes when $a_z(q_z, m) = 0$. From our assumption, it is satisfied when $q_z = 0$, $m = m_0$ but is not for $m < m_0$. Hence, the value of m satisfying $a_z(q_z, m) = 0$ as a function of q_z should have a minimum at $q_z = 0$ (Fig. 6B). It leads to bifurcation into two solutions on the q_z axis as m increases across m_0, and it describes a monopole-antimonopole pair creation of Weyl nodes. Therefore, two Weyl nodes are created at $m = m_0$, and they move along the C_2 axis. We call this case "**1a**."

(iii) C_2 and ΘC_{2y} symmetries

Suppose the wave vector $\mathbf{k}$ is invariant under C_{2z} and ΘC_{2y}. There are two eigenvalues of C_{2z} with opposite signs, yielding two irreps. For (iii-1) $R_c = R_v$, the Hamiltonian satisfies $H(q_x, q_y, q_z, m) = H(-q_x, -q_y, q_z, m) = H^*(q_x, -q_y, q_z, m)$, where "$*$" represents complex conjugation. These equations lead to $a_x = f_x(q_x^2, q_y^2, q_z, m)$, $a_y = q_x q_y f_y(q_x^2, q_y^2, q_z, m)$, and $a_z = f_z(q_x^2, q_y^2, q_z, m)$. As m is increased, it describes creations of

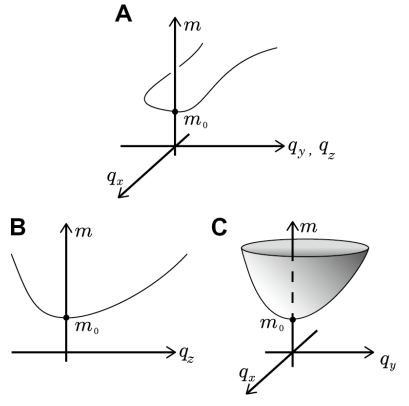

Fig. 6. Values of *m* for closing of the gap as a function of *q*. (**A**) $m = m(q_x, q_y, q_z)$ as a solution of $a_i(q_x, q_y, q_z, m) = 0$ ($i = x, y, z$) in (i). (**B**) $m = m(q_z)$ that satisfies $a_z(0, 0, q_z, m) = 0$ in (ii-2). (**C**) $m = m(q_x, q_y)$ as a solution of $a_z(q_x, q_y, 0, m) = 0$ in (iv-2).

two monopoles and two antimonopoles at $\mathbf{q} = 0$, $m = m_0$. For $m > m_0$, two monopoles are at $(\pm\tilde{q}_x, 0, \tilde{q}_z)$ on the xz plane and two antimonopoles are at $(0, \pm\tilde{q}_y, \tilde{q}'_z)$, where $\tilde{q}_x$, $\tilde{q}_y$, $\tilde{q}_z$, and $\tilde{q}'_z$ depend on m (or the positions of the monopoles and antimonopoles might be exchanged). Notably, in contrast to (ii-1), where the level repulsion prohibits closing of the gap, in the present case (iii-1), the additional ΘC_2 symmetry gives rise to additional constraints and suppresses level repulsion. In our list, this behavior in (iii-1) is represented as **2a**.

For (iii-2) $R_c \neq R_v$, the Hamiltonian satisfies $H(q_x, q_y, q_z, m) = \sigma_z H(-q_x, -q_y, q_z, m)\sigma_z = H^*(q_x, -q_y, q_z, m)$. The similar discussion as in (iii-1) leads to the results $a_x = q_x f_x(q_x^2, q_y^2, q_z, m)$, $a_y = q_y f_y(q_x^2, q_y^2, q_z, m)$, and $a_z = f_z(q_x^2, q_y^2, q_z, m)$. Therefore, for $q_x = q_y = 0$, a_x and a_y identically vanish, and the remaining condition $a_z(0, 0, q_z, m) = 0$ describes a pair creation of Weyl nodes at $\mathbf{q} = 0$ and $m = m_0$ as in (ii-2). It is written as **1a**.

(iv) Mirror symmetry M

Let the z axis denote the direction normal to the mirror plane. Because a square of the mirror operator M is equal to −1 for mirror symmetry or an identity operator times a $\mathbf{k}$-dependent factor for glide symmetry, there are two representations with opposite signs of mirror eigenvalues. For (iv-1) $R_c = R_v$, the Hamiltonian satisfies $H(q_x, q_y, q_z, m) = H(q_x, q_y, -q_z, m)$. This equation is automatically satisfied on the mirror plane $q_z = 0$. Thus, closing of the gap on the mirror plane imposes three conditions $[a_i(q_x, q_y, 0, m) = 0, i = x, y, z]$ for three variables q_x, q_y, and m. This set of equations can have solutions on the mirror plane, and this closing of the gap accompanies a pair creation of Weyl nodes, which will then move symmetrically with respect to the mirror plane. We call this pattern **1sa**.

On the other hand, for (iv-2) $R_c \neq R_v$, we obtained $H(q_x, q_y, q_z, m) = \sigma_z H(q_x, q_y, -q_z, m)\sigma_z$. Hence, within the $q_z = 0$ plane, the Hamiltonian is expressed as $H(q_x, q_z, 0, m) = a_z(q_x, q_y, 0, m)\sigma_z$. Closing of the gap imposes only one condition, $a_z = 0$ (that is, $d_c = 1$), for three variables (q_x, q_y, and m); therefore, the gap can close by changing m. By assumption, the gap-closing condition $a_z(q_x, q_y, 0, m) = 0$ does not have solutions for $m < m_0$, but has a solution at $q_x = q_y = 0$, $m = m_0$. Therefore, the value of m as a function of q_x and q_y has a minimum at $q_x = q_y = 0$, as shown in Fig. 6C. When m is larger than m_0, the gap closes along a loop (nodal line) within the $q_z = 0$ plane. We call this case **1ℓ**.

SUPPLEMENTARY MATERIALS

Supplementary material for this article is available at http://advances.sciencemag.org/cgi/content/full/3/5/e1602680/DC1

Supplementary Text

fig. S1. Trajectories of Weyl nodes after a pair creation at $\mathbf{k}_0$ for representative cases.

fig. S2. Phonon dispersion of HfS.

table S1. Patterns of gap-closing points after parametric gap closing for triclinic and monoclinic space groups.

table S2. Patterns of gap-closing points after parametric gap closing for orthorhombic space groups.

table S3. Patterns of gap-closing points after parametric gap closing for tetragonal space groups.

table S4. Patterns of gap-closing points after parametric gap closing for trigonal and hexagonal space groups.

table S5. Patterns of gap-closing points after parametric gap closing for cubic space groups.

REFERENCES AND NOTES

1. S. Murakami, Phase transition between the quantum spin Hall and insulator phases in 3D: Emergence of a topological gapless phase. *New J. Phys.* **9**, 356 (2007).
2. X. Wan, A. M. Turner, A. Vishwanath, S. Y. Savrasov, Topological semimetal and Fermi-arc surface states in the electronic structure of pyrochlore iridates. *Phys. Rev. B* **83**, 205101 (2011).
3. Z. Wang, Y. Sun, X.-Q. Chen, C. Franchini, G. Xu, H. Weng, X. Dai, Z. Fang, Dirac semimetal and topological phase transitions in A_3Bi (A = Na, K, Rb). *Phys. Rev. B* **85**, 195320 (2012).
4. Z. Wang, H. Weng, Q. Wu, X. Dai, Z. Fang, Three-dimensional Dirac semimetal and quantum transport in Cd_3As_2. *Phys. Rev. B* **88**, 125427 (2013).
5. G. Xu, H. Weng, Z. Wang, X. Dai, Z. Fang, Chern semimetal and the quantized anomalous Hall effect in $HgCr_2Se_4$. *Phys. Rev. Lett.* **107**, 186806 (2011).
6. J. Liu, D. Vanderbilt, Weyl semimetals from noncentrosymmetric topological insulators. *Phys. Rev. B* **90**, 155316 (2014).
7. M. Hirayama, R. Okugawa, S. Ishibashi, S. Murakami, T. Miyake, Weyl node and spin texture in trigonal tellurium and selenium. *Phys. Rev. Lett.* **114**, 206401 (2015).
8. H. Weng, C. Fang, Z. Fang, B. A. Bernevig, X. Dai, Weyl semimetal phase in noncentrosymmetric transition-metal monophosphides. *Phys. Rev. X* **5**, 011029 (2015).
9. S.-M. Huang, S.-Y. Xu, I. Belopolski, C.-C. Lee, G. Chang, B. Wang, N. Alidoust, G. Bian, M. Neupane, C. Zhang, S. Jia, A. Bansil, H. Lin, M. Z. Hasan, A Weyl fermion semimetal with surface Fermi arcs in the transition metal monopnictide TaAs class. *Nat. Commun.* **6**, 7373 (2015).
10. T. Rauch, S. Achilles, J. Henk, I. Mertig, Spin chirality tuning and topological semimetals in strained $HgTe_xS_{1-x}$. *Phys. Rev. Lett.* **114**, 236805 (2015).
11. S.-M. Huang, S.-Y Xu, I. Belopolski, C.-C. Lee, G. Chang, B. Wang, N. Alidoust, G. Bian, M. Neupane, D. Sanchez, H. Zheng, H.-T. Jeng, A. Bansil, T. Neuspert, H. Lin, M. Z. Hasan, A new type of Weyl semimetal with quadratic double Weyl fermions. *Proc. Natl. Acad. Sci. U.S.A.* **113**, 1180–1185 (2016)
12. A. A. Soluyanov, D. Gresch, Z. Wang, Q. S. Wu, M. Troyer, X. Dai, B. A. Bernevig, Type-II Weyl semimetals. *Nature* **527**, 495–498 (2015).
13. H. Weng, C. Fang, Z. Fang, X. Dai, Coexistence of Weyl fermion and massless triply degenerate nodal points. *Phys. Rev. B* **94**, 165201 (2016).
14. S.-Y. Xu, I. Belopolski, N. Alidoust, M. Neupane, G. Bian, C. Zhang, R. Sankar, G. Chang, Z. Yuan, C.-C. Lee, S.-M. Huang, H. Zheng, J. Ma, D. S. Sanchez, B. Wang, A. Bansil, F. Chou, P. P. Shibayev, H. Lin, S. Jia, M. Z. Hasan, Discovery of a Weyl fermion semimetal and topological Fermi arcs. *Science* **349**, 613–617 (2015).
15. B. Q. Lv, H. M. Weng, B. B. Fu, X. P. Wang, H. Miao, J. Ma, P. Richard, X. C. Huang, L. X. Zhao, G. F. Chen, Z. Fang, X. Dai, T. Qian, H. Ding, Experimental discovery of Weyl semimetal TaAs. *Phys. Rev. X* **5**, 031013 (2015).
16. B. Q. Lv, N. Xu, H. M. Weng, J. Z. Ma, P. Richard, X. C. Huang, L. X. Zhao, G. F. Chen, C. E. Matt, F. Bisti, V. N. Strocov, J. Mesot, Z. Fang, X. Dai, T. Qian, M. Shi, H. Ding, Observation of Weyl nodes in TaAs. *Nat. Phys.* **11**, 724–727 (2015).
17. M. V. Berry, Quantal phase factors accompanying adiabatic changes. *Proc. Roy. Soc. A* **392**, 45–57 (1984).
18. G. E. Volovik, *The Universe in a Helium Droplet* (Oxford Univ. Press, 2009).
19. T. Ojanen, Helical Fermi arcs and surface states in time-reversal invariant Weyl semimetals. *Phys. Rev. B* **87**, 245112 (2013).
20. R. Okugawa, S. Murakami, Dispersion of Fermi arcs in Weyl semimetals and their evolutions to Dirac cones. *Phys. Rev. B* **89**, 235315 (2014).
21. F. D. M. Haldane, Attachment of surface "Fermi Arcs" to the bulk Fermi surface: "Fermi-Level Plumbing" in topological metals. arXiv:1401.0529 (2014).
22. A. A. Burkov, M. D. Hook, L. Balents, Topological nodal semimetals. *Phys. Rev. B* **84**, 235126 (2011).
23. K. Mullen, B. Uchoa, D. T. Glatzhofer, Line of Dirac nodes in hyperhoneycomb lattices. *Phys. Rev. Lett.* **115**, 026403 (2015).
24. C. Fang, Y. Chen, H.-Y. Kee, L. Fu, Topological nodal line semimetals with and without spin-orbital coupling. *Phys. Rev. B* **92**, 081201 (2015).
25. Y. Chen, Y. Xie, S. A. Yang, H. Pan, F. Zhang, M. L. Cohen, S. Zhang, Nanostructured carbon allotropes with Weyl-like loops and points. *Nano Lett.* **15**, 6974–6978 (2015).
26. H. Weng, Y. Liang, Q. Xu, R. Yu, Z. Fang, X. Dai, Y. Kawazoe, Topological node-line semimetal in three-dimensional graphene networks. *Phys. Rev. B* **92**, 045108 (2015).
27. Y. Kim, B. J. Wieder, C. L. Kane, A. M. Rappe, Dirac line nodes in inversion-symmetric crystals. *Phys. Rev. Lett.* **115**, 036806 (2015).
28. R. Yu, H. Weng, Z. Fang, X. Dai, X. Hu, Topological node-line semimetal and Dirac semimetal state in antiperovskite Cu_3PdN. *Phys. Rev. Lett.* **115**, 036807 (2015).
29. L. S. Xie, L. M. Schoop, E. M. Seibel, Q. D. Gibson, W. Xie, R. J. Cava, A new form of Ca_3P_2 with a ring of Dirac nodes. *APL Mater.* **3**, 083602 (2015).
30. Y.-H. Chan, C.-K. Chiu, M. Y. Chou, A. P. Schnyder, Ca_3P_2 and other topological semimetals with line nodes and drumhead surface states. *Phys. Rev. B* **93**, 205132 (2016).
31. M. Zeng, C. Fang, G. Chang, Y.-A. Chen, T. Hsieh, A. Bansil, H. Lin, L. Fu, Topological semimetals and topological insulators in rare earth monopnictides. arXiv:1504.03492 (2015).
32. A. Yamakage, Y. Yamakawa, Y. Tanaka, Y. Okamoto, Line-node Dirac semimetal and topological insulating phase in noncentrosymmetric pnictides CaAgX (X = P, As). *J. Phys. Soc. Jpn.* **85**, 013708 (2016).
33. J. Zhao, R. Yu, H. Weng, Z. Fang, Topological node-line semimetal in compressed black phosphorus. *Phys. Rev. B* **94**, 195104 (2016).
34. M. Hirayama, R. Okugawa, T. Miyake, S. Murakami, Topological Dirac nodal Lines in fcc alkaline earth metals. *Nat. Commun.* **8**, 14022 (2017).
35. Z. Zhu, G. W. Winkler, Q. Wu, J. Li, A. A. Soluyanov, Triple point topological metals. *Phys. Rev. X* **6**, 031003 (2016).

36. L. Fu, C. L. Kane, E. J. Mele, Topological insulators in three dimensions. *Phys. Rev. Lett.* **98**, 106803 (2007).
37. J. E. Moore, L. Balents, Topological invariants of time-reversal-invariant band structures. *Phys. Rev. B* **75**, 121306 (2007).
38. C. J. Bradley, A. P. Cracknell, *The Mathematical Theory of Symmetry in Solids: Representation Theory for Point Groups and Space Groups* (Oxford Univ. Press, 2010).
39. S. Murakami, S.-i. Kuga, Universal phase diagrams for the quantum spin Hall systems. *Phys. Rev. B* **78**, 165313 (2008).
40. H. F. Franzen, J. J. Graham, The lower sulphides of hafnium at high temperature. *J. Inorg. Nucl. Chem.* **28**, 377–380 (1966).
41. C. Dagron, F. Thevet, Répartition des types cristallins dans la série des iodosulfures et fluorosulfures des éléments des terres rares et d'yttrium (in French). *C. R. Acad. Sci. Ser. C* **268**, 1867–1869 (1969).
42. H. H. Stadelmaier, W. K. Hardy, Ternäere Kohlenstofflegierungen von Palladium und Platin mit Magnesium, Aluminium, Zink, Gallium, Germanium, Kadmium, Indium, Zinn, Quecksilber, Thallium und Blei (in German). *Z. Metallkd.* **52**, 391–396 (1961).
43. S.-Y. Xu, Y. Xia, L. A. Wray, S. Jia, F. Meier, J. H. Dil, J. Osterwalder, B. Slomski, A. Bansil, H. Lin, R. J. Cava, M. Z. Hasan, Topological phase transition and texture inversion in a tunable topological insulator. *Science* **332**, 560–564 (2011).
44. T. Sato, K. Segawa, K. Kosaka, S. Souma, K. Nakayama, K. Eto, T. Minami, Y. Ando, T. Takahashi, Unexpected mass acquisition of Dirac fermions at the quantum phase transition of a topological insulator. *Nat. Phys.* **7**, 840–844 (2011).
45. K. Ishizaka, M. S. Bahramy, H. Murakawa, M. Sakano, T. Shimojima, T. Sonobe, K. Koizumi, S. Shin, H. Miyahara, A. Kimura, K. Miyamoto, T. Okuda, H. Namatame, M. Taniguchi, R. Arita, N. Nagaosa, K. Kobayashi, Y. Murakami, R. Kumai, Y. Kaneko, Y. Onose, Y. Tokura, Giant Rashba-type spin splitting in bulk BiTeI. *Nat. Mater.* **10**, 521–526 (2011).
46. M. S. Bahramy, B.-J. Yang, R. Arita, N. Nagaosa, Emergence of non-centrosymmetric topological insulating phase in BiTeI under pressure. *Nat. Commun.* **3**, 679 (2012).
47. B.-J. Yang, M. S. Bahramy, R. Arita, H. Isobe, E.-G. Moon, N. Nagaosa, Theory of topological quantum phase transitions in 3D noncentrosymmetric systems. *Phys. Rev. Lett.* **110**, 086402 (2013).

Acknowledgments: We thank S. Ishibashi for providing us with the ab initio code (QMAS) and pseudopotentials. **Funding:** This work is partially supported by Japan Society for the Promotion of Science KAKENHI grant numbers JP26287062, JP26103006, and JP16J08552, and by MEXT (Ministry of Education, Culture, Sports, Science and Technology) Elements Strategy Initiative to Form Core Research Center (Tokodai Institute for Element Strategy). **Author contributions:** All authors contributed to the main contents of this work. S.M. conceived and supervised the project and also did analytical calculations for classifications in terms of the space groups with the help of R.O. M.H. performed the ab initio calculation with contributions from T.M. R.O. also constructed the theory on real materials, such as BiTeI, with the help of S.M. M.H., R.O., and S.M. drafted the manuscript. T.M. gave critical revisions of the manuscript. **Competing interests:** The authors declare that they have no competing interests. **Data and materials availability:** All data needed to evaluate the conclusions in the paper are present in the paper and/or the Supplementary Materials. Additional data related to this paper may be requested from the authors.

Submitted 31 October 2016
Accepted 7 March 2017
Published 12 May 2017
10.1126/sciadv.1602680

Citation: S. Murakami, M. Hirayama, R. Okugawa, T. Miyake, Emergence of topological semimetals in gap closing in semiconductors without inversion symmetry. *Sci. Adv.* **3**, e1602680 (2017).